

Journal of Materials Chemistry A

Accepted Manuscript



This is an *Accepted Manuscript*, which has been through the Royal Society of Chemistry peer review process and has been accepted for publication.

Accepted Manuscripts are published online shortly after acceptance, before technical editing, formatting and proof reading. Using this free service, authors can make their results available to the community, in citable form, before we publish the edited article. We will replace this *Accepted Manuscript* with the edited and formatted *Advance Article* as soon as it is available.

You can find more information about *Accepted Manuscripts* in the [Information for Authors](#).

Please note that technical editing may introduce minor changes to the text and/or graphics, which may alter content. The journal's standard [Terms & Conditions](#) and the [Ethical guidelines](#) still apply. In no event shall the Royal Society of Chemistry be held responsible for any errors or omissions in this *Accepted Manuscript* or any consequences arising from the use of any information it contains.

Cite this: DOI: 10.1039/c0xx00000x

www.rsc.org/xxxxxx

PAPER

Direct synthesis of HZSM-5 from natural clay

Feng Pan^a, Xuchen Lu^{*a,c}, Qingshan Zhu^a, Zhimin Zhang^a, Yan Yan^a, Tizhuang Wang^a and Shiwei Chen^{a,b}

Received (in XXX, XXX) Xth XXXXXXXXX 20XX, Accepted Xth XXXXXXXXX 20XX

DOI: 10.1039/b000000x

Highly crystalline HZSM-5 zeolite was directly synthesized through steam assisted conversion (SAC) approach by using kaolin as raw materials. $\text{NH}_3 \cdot \text{H}_2\text{O}$ was used as alkaline vapor source at the bottom of the teflon. The catalytic performance of the obtained HZSM-5 with $\text{SiO}_2/\text{Al}_2\text{O}_3$ ratios from 25.67 to 80 was investigated for converting methanol to light olefins (MTO). The results indicated that $\text{NH}_3 \cdot \text{H}_2\text{O}$ provided alkalinity to dissolve the raw materials and NH_4^+ cations to balance the charge of the framework. Highly crystalline HZSM-5 with crystal size in the range of 0.8-1 μm could be obtained within 1.0 h at 190 °C. The obtained HZSM-5 possessed high S_{BET} (above 440 m^2/g) and high total pore volume (above 0.3 cm^3/g). The acidity of the HZSM-5 could be affected by $\text{SiO}_2/\text{Al}_2\text{O}_3$ molar ratio and the residual metallic elements (such as Fe, Ti, Ca, P, etc.) in the leached metakaolin. The existence of the metallic elements had the similar effect with the HZSM-5 modified with metal cations. HZSM-5 with higher $\text{SiO}_2/\text{Al}_2\text{O}_3$ molar ratio was favourable for the formation of C2-C4 olefins. The selectivity of C2-C4 olefins reached 68% as the $\text{SiO}_2/\text{Al}_2\text{O}_3$ molar ratio was 68.79. This method avoided exchanging with the ammonium and calcination processes, which not only reduced the cost but also enhanced the productivity obviously.

1. Introduction

As one of the most important zeolites, ZSM-5 has been broadly applied in many important catalytic reactions because of its special pore structure.¹ Therefore, ZSM-5 with nano/micro size has been widely synthesized by using aluminosilicate gel as raw materials in Na^+ -TPA system through hydrothermal method,²⁻⁵ organic solvent system⁶ or without solvent.^{7,8} Consequently, Na^+ ions are still kept in the framework of zeolites for charge compensation. Generally, H-form of the zeolite is usually desired when ZSM-5 is used as a solid acid catalyst. To obtain HZSM-5 catalysts, NaZSM-5 needs to exchange with ammonium salt. Undoubtedly, some problems are inevitable during the ion exchange process, such as increasing the cost, reducing the production efficiency and consuming great energy.

Hence, the direct synthesis of H-ZSM-5 using ammonium hydroxide to replace alkali metal cations might be superior to the conventional methods by eliminating the ion-exchange step. Bibby⁹ successfully synthesized HZSM-5 in NH_4^+ -TPA system without using any alkali metal cations. Hereafter, Ghamam¹⁰ investigated the crystallization kinetics of ZSM-5 as a function of $\text{NH}_4/(\text{NH}_4 + \text{TPA})$, the activation energies for nucleation and crystallization were 9.6 and 15.9 $\text{kcal g}^{-1}\text{mol}^{-1}$, respectively. They concluded that HZSM-5 with different crystal size could be obtained when different silicon sources

and templates were used. When aqueous colloidal silica sol and tetrapropylammonium bromide (TPABr) were adopted as reagents resulted in relatively large single crystals (*ca.* 35 μm). Spherulitic aggregates of very small crystals were obtained as the system contained microfine precipitated silica and tetrapropylammonium hydroxide (TPAOH). Hou et al.¹¹ studied the nucleation and crystal growth of NH_4 -ZSM-5 zeolites in the $(\text{TPA})_2\text{O}-(\text{NH}_4)_2\text{O}-\text{Al}_2\text{O}_3-\text{SiO}_2-\text{H}_2\text{O}$ system by traditional hydrothermal method. They concluded that (a) the rates of amorphous gel dissolution and crystal growth were closely related to the concentration of $[\text{OH}^-]$, (b) the presence of Al_2O_3 and the amount of TPA^+ strongly affected the final crystal size. Recently, Xue¹² directly synthesized NH_4 -ZSM-5 zeolite with nano-sized crystal by introducing seeding suspension. Actually, the synthesis system contained Na^+ ions due to the use of colloidal silica (SiO₂, 30 wt.%; Na₂O, 0.05 wt.%). Moreover, large amount of TPAOH and long crystallization time (96 h) also could not meet the demand of the industry. Therefore, in the aforementioned researches, a large amount of tetrapropylammonium hydroxide (TPAOH) was introduced into the system, and a long time should be spent. In addition, it is necessary to point out that a large amount of effluents with amine was generated because the above mentioned syntheses were performed in hydrothermal system.

Thus, a facile, rapid and economical approach for the direct synthesis of HZSM-5 zeolites is desirable. Generally, ZSM-5

zeolite typically is synthesized by using TEOS or $\text{Na}_2\text{SiO}_3 \cdot 9\text{H}_2\text{O}$ as silicon sources, using organic or inorganic aluminum salts as aluminum sources. Compared with the chemical silicon and aluminum sources, natural clay is considered an economic alternative material for synthesizing zeolites because it is readily available and very economical. Therefore, the conversion of natural clay to highly crystalline ZSM-5 has been gaining much attention.¹³⁻¹⁹

Herein, HZSM-5 zeolites were directly synthesized via steam assisted conversion (SAC) approach. In this method, kaolin clay was adopted as the raw material, $\text{NH}_3 \cdot \text{H}_2\text{O}$ was used as alkaline steam source instead of sodium hydroxide to provide alkalinity. The influence of the amount of ammonia and $\text{SiO}_2/\text{Al}_2\text{O}_3$ ratio on the final products was investigated. Furthermore, the catalytic performance of HZSM-5 with different $\text{SiO}_2/\text{Al}_2\text{O}_3$ molar ratio on the methanol dehydration to olefins (MTO) was investigated. Because the ammonia and the final products were in a state of separation, the filtration step could be omitted. In addition, the residual ammonia at the bottom of the teflon could be recycled, which greatly reduced the emissions of waste liquid.

2. Experimental Section

2.1 Synthesis of HZSM-5

The kaolin (Inner Mongolia, China) was converted to metakaolin by thermal treatment at 1073 K for 2 hr. Then, metakaolin was leached by 6 M HCl solution (solid/liquid ratio 1:5, g/ml) with stirring. After that, the mixture was filtered, washed with deionized water, dried and collected as precursors for the synthesis of HZSM-5.

Table 1 Composition of the leached metakaolin

Conditions	Elemental Content (wt.%)			
	Si	Al	Fe	Ti
80°C, 1 hr	43.01	3.22	0.56	2.05
90°C, 1 hr	43.91	2.26	0.32	1.46
90°C, 2 hr	44.55	1.46	0.14	1.22
90°C, 4 hr	44.95	1.20	0.06	0.72

Note: the data was obtained on a X-ray fluorescence spectrometer (AXIOS, PANalytical B.V.)

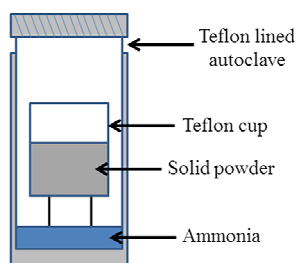


Fig. 1 Schematic diagram of the reaction vessel used for synthesis of HZSM-5 by Steam-Assisted Conversion (SAC)

Dealuminated metakaolin was uniformly mixed with

TPAOH in the molar ratios $\text{SiO}_2 : \text{Al}_2\text{O}_3 : \text{TPAOH} : \text{H}_2\text{O}$ (only came from TPAOH solution) = 1 : 0.0389 ~ 0.0125 : 0.052 : 2.08. The mixture was placed in a special autoclave where ammonia was used as a source of steam at the bottom of the teflon (Fig. 1). Crystallization of the mixture was performed under autogenous pressure and at 190 °C. HZSM-5 was obtained by removing the organic template at 550 °C for 6 hr.

2.2 Characterization

Powder XRD patterns of the dried solid products were recorded on a PANalytical X'pert diffractometer with CuK α radiation. The morphology and chemical composition of the samples were characterized by field-emission scanning electron microscopy (SEM) (JEM-7001F, JEOL, Japan). N_2 adsorption-desorption were measured on AUTOSORB-1 analyzer (Quantachrome). Prior to measurement, the samples were degassed at 573 K for 10 hr under vacuum. Total acidity and acid strength distribution of the catalyst were determined by calorimetric measurement of differential adsorption of NH_3 at 60 °C and subsequent TPD of the adsorbed NH_3 with a ramp of 10 °C min^{-1} up to 700 °C (Quantachrome CHEMBET 3000, USA). The coke amount was determined using a TG/DTA6300 (Japan) thermogravimetric analyzer from 30 to 800°C under air flow with a heating rate of 10°C/min. Pyridine adsorption followed by infrared (IR) spectroscopy (Nicolet Magna FTIR 550 spectrometer) was used to investigate the acid sites at 423 K. Samples of fresh catalysts were first pressed into thin wafers and activated *in situ* in the IR cell under secondary vacuum (10^{-6} mbar) at 623 K. The extinction coefficients used for the estimation of the Brønsted and Lewis acid sites were the ones previously determined by Guisnet et al.²⁰: 1.13 $\text{cm} \mu\text{mol}^{-1}$ and 1.28 $\text{cm} \mu\text{mol}^{-1}$ for Brønsted and Lewis acidities, respectively. The concentration of different acid sites is calculated from the following formula (Beer-Lambert's law)²¹:

$$C = \frac{A}{\epsilon} \times \frac{S}{m} \times 100$$

Where C is the concentration of acid sites ($\mu\text{mol g}^{-1}$), A is the area of band (cm^{-1}), S is the surface of the wafer (2 cm^2), ϵ is the molar extinction coefficient ($\text{cm} \mu\text{mol}^{-1}$), and m is the mass of sample (mg).

2.3 Catalytic performances

Catalytic reaction tests were conducted at 400 °C under atmospheric pressure in a conventional continuous down flow, fixed-bed stainless steel reactor (inner diameter 6 mm). 0.3 g of HZSM-5 catalyst (40-60 mesh) was placed in the center zone of the reactor. Prior to the catalytic measurements, the fresh catalyst was activated at 500 °C for 2 hr with nitrogen (15 mL min^{-1}). Then, reactant (50 vol% methanol solution) was pumped into pre-heater reactor through a piston pump (WHSV of methanol was 6.67 h^{-1}), and got into reactor with nitrogen (15 mL min^{-1}).

The feed and products were analyzed on-line by gas chromatography (SHIMADZU GC-2014) equipped with flame

ionization detector (FID) and thermal conductivity detector (TCD). FID with a TG-BOND capillary column (50 m × 0.32 mm × 15 μm, Thermo, USA) analyzed un-reacted methanol, dimethyl ether and hydrocarbons (C1-C5). TCD with a GDX-101 packed column detected CO, H₂ and CO₂. All products were identified according to the standard gases (Beijing Gaisi Chemical Gases Center), and the concentration of the components in the reactor effluent steam, expressed as molar percentages, was determined from the on-line chromatographic results. The response factors in gas chromatography analysis were evaluated from the effective carbon number. In addition, the conversion of methanol to coke was neglected because the instantaneous formation of coke was dependent on reaction time and difficult to estimate. The conversion of methanol was calculated by applying the molar balance between the inlet and outlet of the reactor. Selectivity for the products of interest were expressed as mass percentage of each product and calculated according to the carbon balance between the inlet and the outlet of the reactor.

3. Results and discussion

3.1 The role of NH₃·H₂O

To investigate the role of NH₃·H₂O, a series experiments were performed with different aqueous ammonia content at the bottom of the teflon.

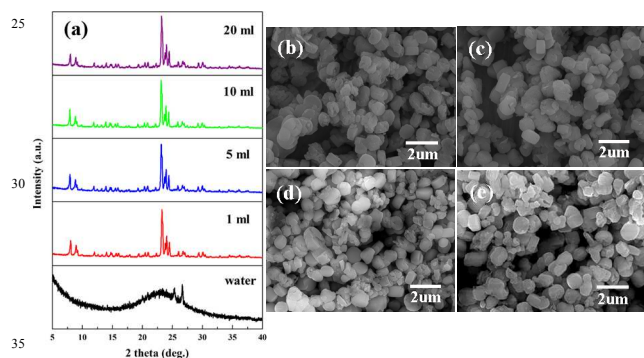


Fig. 2 XRD patterns (a) and SEM images of HZSM-5 obtained with different ammonia content at the bottom of the teflon (b) 1 ml; (c) 5 ml; (d) 10 ml; (e) 20 ml.

XRD patterns of the samples obtained with different ammonia content are shown in Fig. 2. No characteristic diffraction peaks of MFI were detected when the water was adopted as steam source at the bottom of the teflon. On the contrary, strong diffraction peaks of MFI (JCPDS Card No.00-037-0359) appeared as the content of ammonium hydroxide was only 1 ml, indicating highly crystalline HZSM-5 could be obtained by using NH₃·H₂O as steam source. As could be seen in Fig. 2 (b), HZSM-5 showed uniform columned shapes with the crystal size of ca. 800 nm (axis *a* × *c*: 800 ~ 1000 nm × 300 ~ 400 nm). Highly crystalline HZSM-5 was still obtained as continued to increase the content of NH₃·H₂O. However, the content of NH₃·H₂O had no significant influence on the crystal sizes of the final products. Therefore, HZSM-5 with high crystallinity could be obtained in a wide range of

NH₃·H₂O when NH₃·H₂O was used as alkaline steam source at the bottom of the teflon.

Possibly, the amount of NH₃·H₂O only affects the crystallization rate. To prove this hypothesis, the materials were treated for different times at 190 °C with 1 ml and 20 ml NH₃·H₂O, respectively. As illustrated in Fig. 3, highly crystalline HZSM-5 could be obtained within 1.0 h as the content of NH₃·H₂O was 20 ml. The results indicated that the amount of alkaline steam source significantly influenced the rate of crystallization.

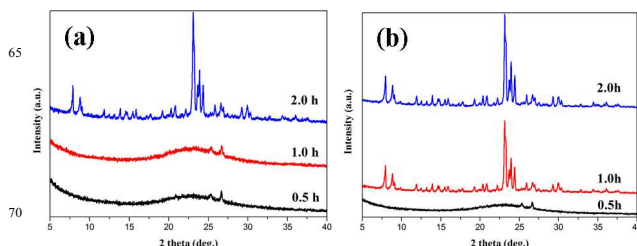


Fig. 3 XRD patterns of HZSM-5 obtained at different times with different ammonia content (a) 1 ml; (b) 20 ml.

The above results indicated that the NH₃·H₂O played a vital role for the formation of HZSM-5. As we all know, NH₃·H₂O becomes NH₃ and H₂O vapor rather than directly dissociates into NH₄⁺ and OH⁻ when it is heated. Due to the strong adsorption performance of the kaolinite,^{22, 23} NH₃ and H₂O vapor was absorbed on the surface of kaolinite or among the layers, and ionized into NH₄⁺ and OH⁻ ions. Thus, the NH₃·H₂O provided alkalinity for the dissolution of the raw materials and NH₄⁺ ions to balance the charge of the framework. In addition, the crystallization rate was improved significantly by using steam assisted conversion (SAC) approach. This phenomenon might be attributed to the acceleration of the polycondensation reactions of silicon aluminum species under alkaline steam environment, and the promotion of mass transfer of silicon aluminium species around the nucleus.

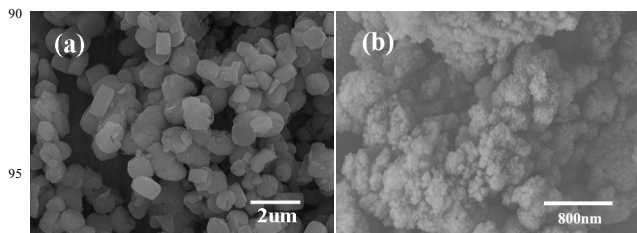


Fig. 4 SEM images of the samples obtained with (a) NH₃·H₂O and (b) NaOH

Compared with the reference,⁹ the crystal size was significantly reduced to submicron grade, and the crystallization time could be shortened to 1.0 hr. However, it was worth noting that no nano-sized HZSM-5 could be obtained when used NH₃·H₂O as steam source. To discuss the different characteristics between NH₃·H₂O and NaOH, a contrast sample was synthesized by adding NaOH to provide basicity, and using water to replace NH₃·H₂O at the bottom of the teflon. As showed in Fig. 4, nano-sized ZSM-5 crystals

were formed as NaOH was contained in the system. This result might be ascribed to the significant difference of the hydration ability of Na^+ and HN_4^+ ions.^{24, 25} Generally, HN_4^+ ions have lower ability of coagulation and hydration, which can hamper the formation of crystal nucleus and reduce the crystallization rate.^{26, 27} As a result, no nano-sized HZSM-5 could be obtained.

In order to verify the ammonium ions were involved in the balance of skeleton charge, the samples obtained with different content of $\text{NH}_3 \cdot \text{H}_2\text{O}$ were analyzed on a thermogravimetric analyzer. Fig. 5 shows the TG-DTG curves of the samples obtained with different ammonia content and NaOH. Both NH_4^+ and TPA^+ cations can get into the samples to compensate the negative charge of the framework. According to the curves, two endothermic peaks at 350-450 °C and 450-500 °C were observed when adopted $\text{NH}_3 \cdot \text{H}_2\text{O}$ as alkaline steam. The formation of the peaks were attributed to the decomposition of TPA^+ at 350-450 °C⁹ and the release of NH_3 at 450-500 °C,¹² respectively.

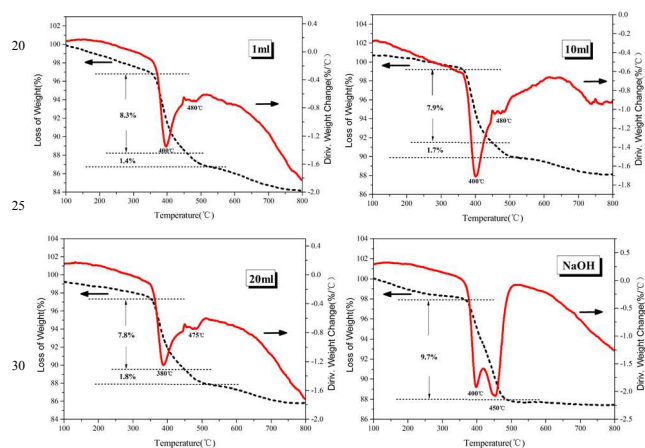


Fig. 5 TG-DTG curves of samples obtained with different amount of ammonia and the sample obtained by using NaOH as alkali source

The decomposition temperature of TPA^+ was much higher than that reported by Cai,²⁸ which demonstrated that the TPA^+ ions got into the pore channels and frameworks via combining with silicon and aluminum species. The weight loss of TPA^+ was 8.3%, 7.7% and 7.8%, and that of NH_4^+ was 1.4%, 1.7% and 1.8% when the content of ammonium hydroxide was 1 ml, 10 ml and 20 ml, respectively. The results clearly showed that the content of NH_4^+ got into the skeleton increased with the increase of $\text{NH}_3 \cdot \text{H}_2\text{O}$. In contrast, the amount of TPA^+ ions involved into the balance of framework charge decreased with the increase of $\text{NH}_3 \cdot \text{H}_2\text{O}$. Consequently, the amount of NH_4^+ and TPA^+ that got into the framework to balance the charge was constant as the $\text{SiO}_2/\text{Al}_2\text{O}_3$ ratio was fixed. No endothermic peak at 450-500 °C was observed in the TG-DTG curve as the sample was synthesized with NaOH. However, the total loss weight was close to that of the samples obtained under the ammonia steam environment. Therefore, it was worth recalling that the absorbed NH_3 and H_2O decomposed into NH_4^+ and OH^- ions, and the NH_4^+ got into the framework to balance the charge.

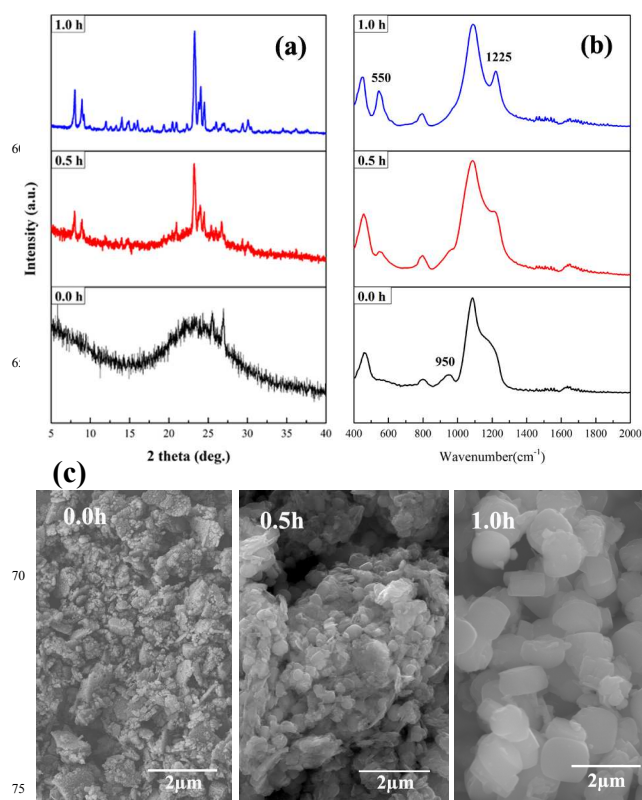


Fig. 6 XRD patterns (a), IR spectra (b) and SEM images (c) of the sample obtained at different times

Note: 10 ml $\text{NH}_3 \cdot \text{H}_2\text{O}$ was placed at the bottom of the teflon

To investigate the formation process of HZSM-5, the change of the structures and morphology were characterized. According to the XRD patterns, for the initial sample only a broad and flat diffraction band at $2\theta = 15\text{-}38^\circ$ could be observed, which demonstrated that the sample was amorphous phase. After treated for 0.5 hr, the characteristic diffraction peaks of HZSM-5 at $2\theta = 7\text{-}9^\circ$, $22\text{-}25^\circ$ began to appear (Fig. 6 (a)), and the characteristic band of the five-membered ring at about 550 cm^{-1} emerged in the IR spectra (Fig. 6 (b)). When crystallization time increased to 0.5 hr, the amorphous aluminosilicates completely disappeared, and pure submicron ZSM-5 was obtained, as could be seen in the SEM image (Fig. 6 (c)). It was clear that the sample exhibited intensive diffraction peaks at $2\theta = 7\text{-}9^\circ$, $22\text{-}25^\circ$ as the crystallization increased to 1.0 hr, which was typical structure of HZSM-5. The characteristic band of the five-membered ring at about 550 cm^{-1} could be seen clearly in the spectra of HZSM-5. Furthermore, the peak at 1225 cm^{-1} was formed, which assigned to the asymmetric stretch vibration of the T-O bond.

3.2 The role of $\text{SiO}_2/\text{Al}_2\text{O}_3$ molar ratio

Fig. 7 shows the XRD patterns of the directly synthesized HZSM-5 samples with different $\text{SiO}_2/\text{Al}_2\text{O}_3$ ratios. All samples exhibited resolved peaks corresponding to the MFI structure without any detectable impurities. It is well known that the Si-O bond (0.161 nm) is shorter than the Al-O bond (0.175 nm),^{29, 30} which caused the shrinkage of crystal cell and the

decrease of crystal face distance.^{31, 32} As a result, the peaks at $2\theta = 22\text{-}25^\circ$ gradually shifted to higher diffraction angles as the $\text{SiO}_2/\text{Al}_2\text{O}_3$ increased.

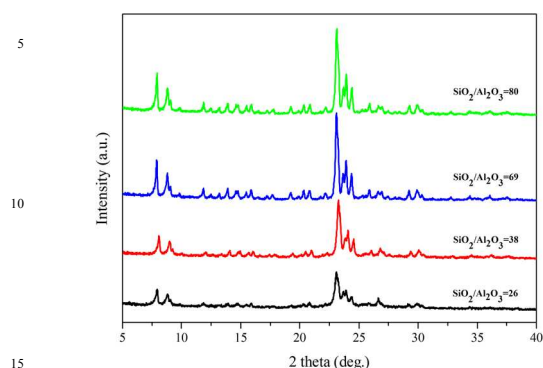


Fig. 7 XRD patterns of the samples synthesized from leached kaolin with different $\text{SiO}_2/\text{Al}_2\text{O}_3$ ratio

However, the diffraction peaks of the sample ($\text{SiO}_2/\text{Al}_2\text{O}_3 = 26$) were much broader than that of the others, the result indicated that either the relative crystallinity was low or the crystal size was nanoscale. According to the N_2 adsorption/desorption results, the S_{BET} of the sample ($\text{SiO}_2/\text{Al}_2\text{O}_3 = 26$) was only $287.3 \text{ m}^2 \cdot \text{g}^{-1}$, demonstrating the crystallinity was poor. The result was in agreement with that reported by Xue.³³ Higher aluminate content hindered the increase of the single silicate ions that were necessary for the formation of crystal nuclei. In addition, more framework aluminum needed more cations to balance the negative charge of the skeleton, which lowered the crystallization rate.³⁴ HZSM-5 with crystallinity ca. 95.5% could be successfully synthesized as $\text{SiO}_2/\text{Al}_2\text{O}_3$ was 38, the S_{BET} and micropore area were as high as $439.8 \text{ m}^2 \cdot \text{g}^{-1}$ and $291.7 \text{ m}^2 \cdot \text{g}^{-1}$, respectively (Table 2). No obvious change could be observed as $\text{SiO}_2/\text{Al}_2\text{O}_3$ continued increasing to 80. Therefore, the raw material with higher $\text{SiO}_2/\text{Al}_2\text{O}_3$ ratio was beneficial to fast converting to highly crystalline HZSM-5 by steam-assisted conversion (SAC) method.

Table 2 Porous properties of ZSM-5 with different $\text{SiO}_2/\text{Al}_2\text{O}_3$ molar ratio

Property	$\text{SiO}_2/\text{Al}_2\text{O}_3$ molar ratio			
	26	38	69	80
Total surface area / ($\text{m}^2 \cdot \text{g}^{-1}$) ^a	287.3	439.8	440.4	445.4
Micropore area / ($\text{m}^2 \cdot \text{g}^{-1}$) ^b	171.4	291.7	293.1	305.4
External surface area / ($\text{m}^2 \cdot \text{g}^{-1}$) ^b	115.8	148.1	147.3	140.0
Pore volume / ($\text{cm}^3 \cdot \text{g}^{-1}$) ^c	0.21	0.30	0.32	0.32
Micropore volume / ($\text{cm}^3 \cdot \text{g}^{-1}$) ^b	0.08	0.13	0.13	0.14
Micropore pore diameter / nm ^d	0.55	0.55	0.55	0.55

a - Determined by BET method from $P/P_0 = 0.02\text{-}0.07$

b - Determined by t-plot method from $P/P_0 = 0.4\text{-}0.6$

c - Calculated at $P/P_0 = 0.99$

d - Determined by HK method

As illustrated in the SEM images (Fig. 8), some amorphous flaky material could be observed in the final product when $\text{SiO}_2/\text{Al}_2\text{O}_3$ was 26, which coincided with the XRD and N_2

adsorption/desorption results. The morphology of HZSM-5 was uniform columned structure (axis $a \times c: 1 \mu\text{m} \times 600 \text{ nm}$) as the $\text{SiO}_2/\text{Al}_2\text{O}_3$ was in the range of 38~80. It could be concluded that there was no significant effect on the morphology and crystal size of HZSM-5 just only changed the $\text{SiO}_2/\text{Al}_2\text{O}_3$ molar ratio. Inversely, as reported in some references,^{33, 35} the crystal size increased with the increase of $\text{SiO}_2/\text{Al}_2\text{O}_3$. The significant difference might be caused by the vast different properties between clay minerals and chemical raw materials.

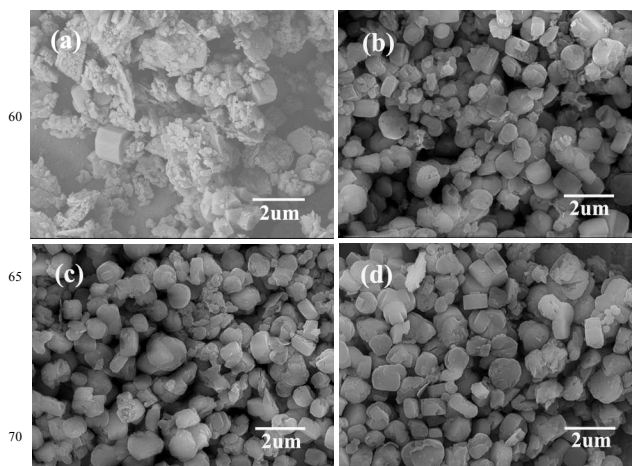


Fig. 8 SEM images of the samples synthesized from leached kaolin with different $\text{SiO}_2/\text{Al}_2\text{O}_3$ ratio (a) $\text{SiO}_2/\text{Al}_2\text{O}_3=26$; (b) $\text{SiO}_2/\text{Al}_2\text{O}_3=38$; (c) $\text{SiO}_2/\text{Al}_2\text{O}_3=69$; (d) $\text{SiO}_2/\text{Al}_2\text{O}_3=80$

3.3 Acidity of the samples with different $\text{SiO}_2/\text{Al}_2\text{O}_3$ ratio

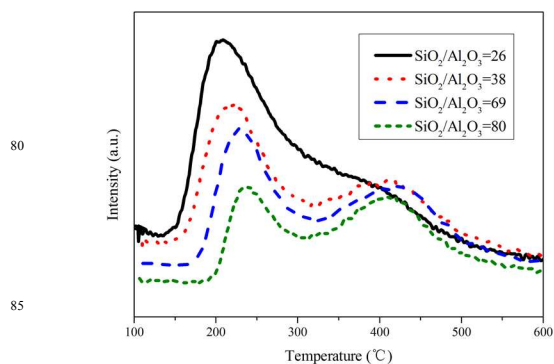


Fig. 9 NH_3 -TPD curves of the obtained samples with different $\text{SiO}_2/\text{Al}_2\text{O}_3$ molar ratio

Fig. 9 gives the NH_3 -TPD curves of the obtained HZSM-5 samples with different $\text{SiO}_2/\text{Al}_2\text{O}_3$ molar ratio. All samples showed a typical NH_3 -TPD spectrum with two peaks at 200-300 °C and 350-500 °C, corresponding to NH_3 eluted from the weak and strong acid sites, respectively. Peak at lower temperature is assigned to the connection between H bonds and O-Si bonds of the weak acid center and non-acid center. Peak at higher temperature stands for the strong acid center that is related with the Al atoms.³⁶ The results indicated that the increase of the $\text{SiO}_2/\text{Al}_2\text{O}_3$ molar ratio led to a decrease both in the number of weak and strong acid sites, especially the weak acid sites. The desorption temperature corresponding

to both the strong acid sites and weak acid sites moved towards higher temperature as the $\text{SiO}_2/\text{Al}_2\text{O}_3$ increased to 69, suggesting that the acid strength increased slightly. However, a shift to lower temperature for strong acidic sites was observed as the $\text{SiO}_2/\text{Al}_2\text{O}_3$ ratio further increased to 80, corresponding to a decline in the strength of the strong acidity. The results obtained by chemical titration (Table 3) well agreed with the curves. Two reasons might be ascribed to the lower content of strong acidity in the sample with low $\text{SiO}_2/\text{Al}_2\text{O}_3$ ($\text{SiO}_2/\text{Al}_2\text{O}_3 = 26$): some Al species could not coordinate with Si to form MFI structures, which caused the poor crystallinity of the final product. This conclusion was proved by the XRD and N_2 desorption results. In addition, some metallic ions such as Fe^{2+} , Ti^{2+} retained in the leached metakaolin have got into the framework during the crystallization. As could be seen the results of energy dispersive spectrum analysis (EDSA) (Fig.10). Generally, M^{2+} can get into the framework by exchanging with H^+ from strong acid sites, and produce one weak acidity by polarization.³⁷ As a result, the weak acid sites were enhanced, but the strong acidity almost disappeared when the $\text{SiO}_2/\text{Al}_2\text{O}_3$ was 26.

Table 3 Acidity of the synthesized HZSM-5 with different $\text{SiO}_2/\text{Al}_2\text{O}_3$ molar ratio

$\text{SiO}_2/\text{Al}_2\text{O}_3$ molar ratio	Acidity (NH_3 , mmol/g)		
	Weak acidity	Strong acidity	Total
26	0.90	0.07	0.97
38	0.63	0.24	0.85
69	0.51	0.21	0.72
80	0.39	0.18	0.57

Note: weak acidity: from 373 to 643 K; strong acidity: from 643 to 823 K. both the weak and strong acidity were quantified by titration.

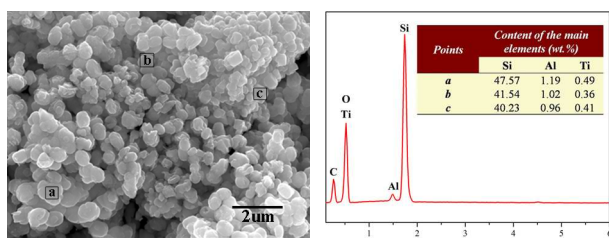


Fig.10 SEM-EDS results of the sample ($\text{SiO}_2/\text{Al}_2\text{O}_3=38$)

The Brønsted acid (B acid) and Lewis acid (L acid) were analyzed by Py-IR adsorption (Fig. 11). The amount of two kinds of acids was calculated according to the Beer-Lambert's law and shown in Table 4. As could be seen in the curves, the intensity of the peak at about 1547 cm^{-1} belongs to Brønsted acid sites gradually increased as the $\text{SiO}_2/\text{Al}_2\text{O}_3$ increased. Inversely, the peak at 1455 cm^{-1} corresponding to the Lewis acid sites decreased markedly as the $\text{SiO}_2/\text{Al}_2\text{O}_3$ increased from 26 to 80. The variation tendency of B acid and L acid was significant different from the reported documents,^{38, 39} which might be ascribed to the different properties between natural clay and chemical materials. As stated and proved by EDS results previously, the M^{2+} (such as Fe, Ti, Ca, P, etc.)

could get into the framework. Thus, in this system, the Brønsted acid sites could be partially neutralized by these M^{2+} cations. Furthermore, the extra-framework aluminium could give rise to Lewis acidity in low temperature regions. Consequently, the sample with lower $\text{SiO}_2/\text{Al}_2\text{O}_3$ molar ratio contained higher content of the Lewis acidity. The bands at about 1490 cm^{-1} , which represents a mix of Brønsted and Lewis acidity,^{39, 40} revealed a gradual increase of the intensity by reducing the aluminum content. The results were good agreement with that reported in the references.²¹ Finally, the band at 1610 cm^{-1} is generally assigned to the physical adsorbed pyridine due to the combination of hydrogen bonds and surface hydroxyl.^{40, 41}

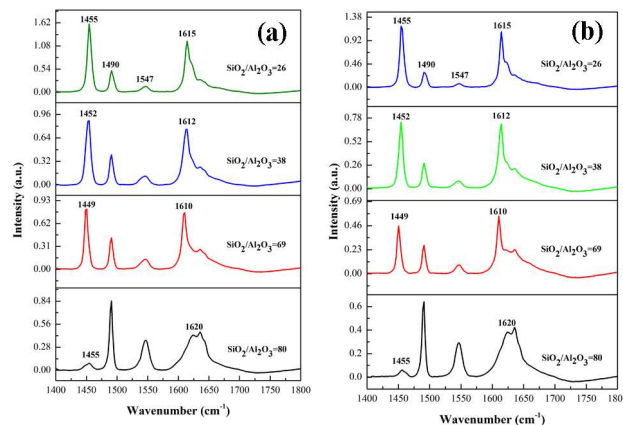


Fig.11 FT-IR spectra of pyridine adsorbed on ZSM-5 with different $\text{SiO}_2/\text{Al}_2\text{O}_3$ molar ratios desorption temperature: (a) 250 °C, (b) 450 °C.

Table 4 Amount of the Brønsted acid and Lewis acid of as-synthesized HZSM-5 with different $\text{SiO}_2/\text{Al}_2\text{O}_3$

$\text{SiO}_2/\text{Al}_2\text{O}_3$ molar ratio	250°C			450°C				
	L	B	Total	L/B	L	B	Total	L/B
26	96.9	5.8	102.7	16.7	71.4	4.2	75.6	17.0
38	88.4	11.1	99.5	7.9	63.2	7.9	71.1	8.0
69	79.5	10.9	90.4	7.3	58.5	7.2	65.7	8.1
80	37.9	20.1	58.0	1.8	26.2	13.2	39.4	2.0

Note: L stands for Lewis acid; B stands for Brønsted acid. Unit: $\mu\text{mol/g}$

3.4 Catalytic performances for MTO reaction

To investigate the influence of $\text{SiO}_2/\text{Al}_2\text{O}_3$ molar ratio on the catalytic performance, the four samples were tested on a fixed-bed stainless steel reactor. The reaction conditions were as follows: reaction temperature, 673K; WHSV: 6.67 h^{-1} ; atmospheric pressure; methanol concentration, 50% (V/V).

As illustrated in Fig. 12, the catalytic activity and products selectivity of the HZSM-5 with different $\text{SiO}_2/\text{Al}_2\text{O}_3$ ratio exhibited significant difference. The conversion of methanol on HZSM-5 (26) began to decrease when continuously reacted for 23 hr. In contrast, the conversion of methanol on the samples with higher $\text{SiO}_2/\text{Al}_2\text{O}_3$ ratio was still over 95% after continuously reacted for 72 hr. As stated by previous researchers,⁴²⁻⁴⁵ the hydrogen transfer and isomerization

reactions could be restrained because the amount of both strength acid and weak acid decreased with the increase of $\text{SiO}_2/\text{Al}_2\text{O}_3$ molar ratio. Moreover, ethylene and propylene can be generated through the cracking reactions of the advanced hydrocarbons. Consequently, the selectivity of ethylene and propylene on HZSM-5 (69) was higher than that on HZSM-5 (38), as could be seen in Fig. 12 (b) and (c). Most of the researchers claimed that the strong acid sites are responsible for the formation of olefins.^{46, 47} Thus, due to the lower content of strong acid, the selectivity to C2-C4 olefins on HZSM-5 (26) was only 45%, and decreased quickly as prolonged the reaction time. In contrast, the selectivity of C2-C4 olefins on the HZSM-5 with higher $\text{SiO}_2/\text{Al}_2\text{O}_3$ ratio began to decrease after running for a long time. The selectivity of C2-C4 olefins significantly increased to 68% as the $\text{SiO}_2/\text{Al}_2\text{O}_3$ increased to 69. Nevertheless, the weak acid and strong acid reduced as the $\text{SiO}_2/\text{Al}_2\text{O}_3$ ratio continued to increasing to 80, which caused the decrease of C2-C4 olefins dramatically.

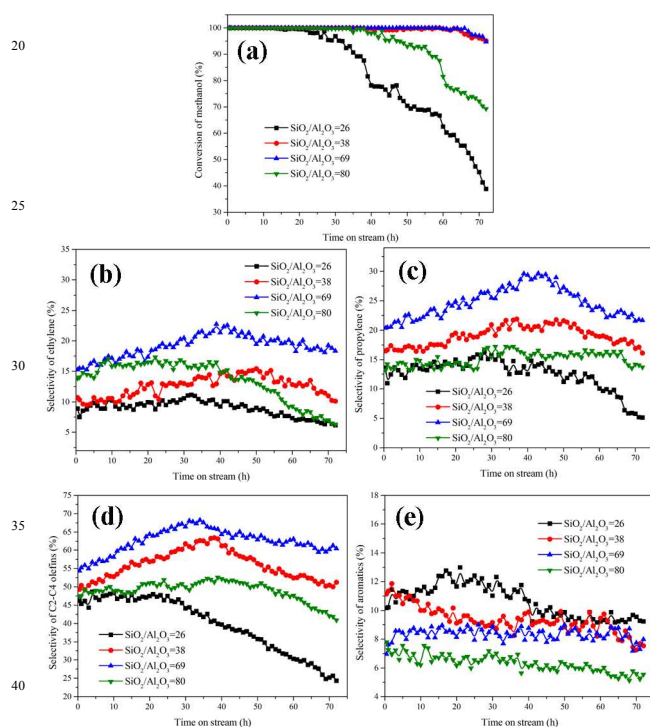


Fig.12 Conversion of methanol (a); selectivity of ethylene (b); selectivity of propylene (c); selectivity of C2-C4 olefins (d) and selectivity of aromatics (e) on ZSM-5 with different $\text{SiO}_2/\text{Al}_2\text{O}_3$ molar ratio as a function of time-on-stream

As stated previously, the retained metallic elements could get into the framework, change the acid strength and density, which also contributed to enhancing the olefins selectivity. Therefore, it could be concluded that the suitable acid strength can improve the selectivity of C2-C4 olefins. It has been proven that the increase in aluminium content causes an increase in aromatic selectivity, and a decrease in olefin selectivity.^{48, 49} Thus, it could be seen that the increase in aluminium content caused an increase in aromatic selectivity

(Fig. 12 (e)), which was consistent with that of reported by previous researchers.

Carbon deposition inevitably occurs during the reaction process, which can reduce the acid strength, acid density, and the pore size of the HZSM-5 zeolites. Hence, proper amount of carbon deposition is beneficial for the formation of light olefins.⁵⁰ Nevertheless, a large amount of carbon will generate a negative effect for the catalytic reactions. To estimate the amount and rate of carbon deposition on the catalyst, the reacted HZSM-5 catalysts were analyzed by TG analyzer. As could be seen in the TG curves (Fig. 13), the amount of deposited carbon decreased gradually as the $\text{SiO}_2/\text{Al}_2\text{O}_3$ ratio increase to 69. In addition, an obvious small peak at 450 °C could be observed clearly in all curves, indicating the types of deposited carbon on the four samples at low temperature were similar. Another peak at the higher temperature zone gradually shifted to the lower temperature as increasing the $\text{SiO}_2/\text{Al}_2\text{O}_3$ ratio to 80, which might be attributed to the type of the long chain hydrocarbons changed. Moreover, the areas of the peak 75 also gradually reduced, demonstrating the content of the aromatics or advanced hydrocarbons decreased.

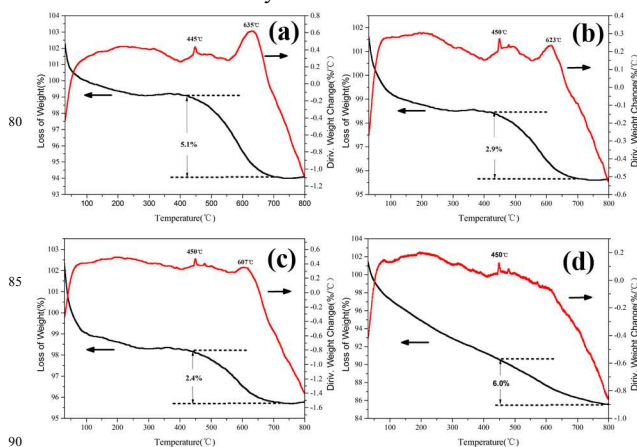


Fig. 13 TG curves of the reacted samples with different $\text{SiO}_2/\text{Al}_2\text{O}_3$ ratio (a) $\text{SiO}_2/\text{Al}_2\text{O}_3=26$; (b) $\text{SiO}_2/\text{Al}_2\text{O}_3=38$; (c) $\text{SiO}_2/\text{Al}_2\text{O}_3=69$; (d) $\text{SiO}_2/\text{Al}_2\text{O}_3=80$

Therefore, HZSM-5 zeolites with appropriate concentration and strength of acid sites can be achieved by controlling the leaching conditions, which is crucial for catalytic performance of the obtained HZSM-5 catalysts.

Conclusions

Highly crystalline HZSM-5 zeolite was directly synthesized through steam assisted conversion (SAC) approach by using kaolin as raw materials. Because Fe, Ti, P, Ca elements could be introduced into the final products naturally, HZSM-5 synthesized from kaolin showed good stability and anti-carbon deposition. The $\text{SiO}_2/\text{Al}_2\text{O}_3$ ratio could significantly influence the catalytic performance of the obtained HZSM-5 catalysts. Some features of this work are as follows: (1) The leached metakaolin could not be treated with gelation and aging before crystallization. (2) HZSM-5 can be directly synthesized within 1.0 hr, which is shortened 22 times compared with the value

reported in the document. (3) The crystal size can be reduced to submicron level (0.8-1.0 μm), which is much smaller than that reported in the reference (ca. 35 μm). (4) We have adopted $\text{NH}_3\cdot\text{H}_2\text{O}$ as alkaline steam source instead of sodium hydroxide to provide alkalinity and NH_4^+ ions that participate the balance of the framework charge. In addition, this method provided an easy and effective path for the synthesis of HZSM-5zeolites. Therefore, it may be a general way to produce different H-type zeolites by using chemical raw materials or natural minerals.

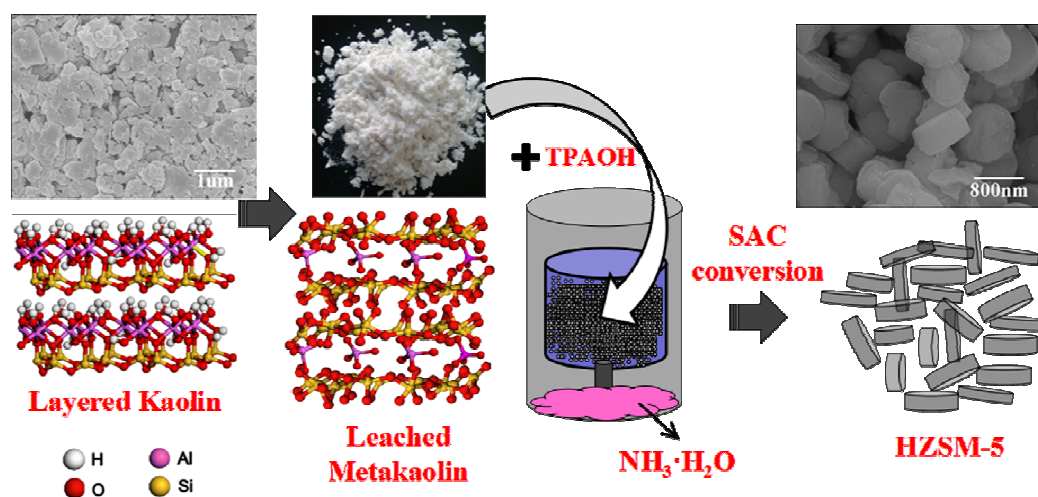
Notes and references

- ^a State Key Laboratory of Multiphase Complex Systems, Institute of Process Engineering, Chinese Academy of Sciences, No. 1 Bei-er-tiao, Zhong-guan-cun, Haidian District, Beijing 100190, P. R. China. Tel: +86 10 8254 4889; E-mail: xclu@home.ipe.ac.cn
- ^b University of Chinese Academy of Sciences, Beijing 100039, PR China
- ^c United Research Center for Resource and Materials, Wuhai 016000, PR China
- † Electronic Supplementary Information (ESI) available: [details of any supplementary information available should be included here]. See DOI: 10.1039/b000000x/
- ‡ Footnotes should appear here. These might include comments relevant to but not central to the matter under discussion, limited experimental and spectral data, and crystallographic data.
- C. S. Cundy and P. A. Cox, *Chem. Rev.*, 2003, **103**, 663-702.
 - M. Ali, B. Brisdon and W. Thomas, *Appl. Catal., A*, 2003, **252**, 149-162.
 - L. Tosheva and V. P. Valtchev, *Chem. Mater.*, 2005, **17**, 2494-2513.
 - D. P. Serrano, J. Aguado, J. M. Escola, J. M. Rodríguez and Á. Peral, *Chem. Mater.*, 2006, **18**, 2462-2464.
 - G. Majano, A. Darwiche, S. Mintova and V. Valtchev, *Ind. Eng. Chem. Res.*, 2009, **48**, 7084-7091.
 - G. T. Vuong and T. O. Do, *J. Am. Chem. Soc.*, 2007, **129**, 3810-3811.
 - L. Ren, Q. Wu, C. Yang, L. Zhu, C. Li, P. Zhang, H. Zhang, X. Meng and F.-S. Xiao, *J. Am. Chem. Soc.*, 2012, **134**, 15173-15176.
 - K. Shen, W. Qian, N. Wang, C. Su and F. Wei, *J. Am. Chem. Soc.*, 2013, **135**, 15322-15325.
 - D. Bibby, N. Milestone and L. Aldridge, *Nature*, 1980, **285**, 30-31.
 - M. Ghamami and L. Sand, *Zeolites*, 1983, **3**, 155-162.
 - L. Y. Hou, L. B. Sand and R. W. Thompson, *Stud. Surf. Sci. Catal.*, 1986, **28**, 239-246.
 - T. Xue, Y. M. Wang and M. Y. He, *Microporous Mesoporous Mater.*, 2012, **156**, 29-35.
 - S. M. Holmes, S. H. Khoo and A. S. Kovo, *Green Chem.*, 2011, **13**, 1152-1154.
 - K. Shen, W. Qian, N. Wang, J. Zhang and F. Wei, *J. Mater. Chem.*, 2013, **1**, 3272-3275.
 - H. Katsuki, S. Furuta and S. Komarneni, *J. Am. Ceram. Soc.*, 2000, **83**, 1093-1097.
 - F. Pan, X. Lu, Y. Wang, S. Chen, T. Wang and Y. Yan, *Microporous Mesoporous Mater.*, 2014, **184**, 134-140.

- F. Pan, X. Lu, Y. Wang, S. Chen, T. Wang and Y. Yan, *Mater. Lett.*, 2014, **115**, 5-8.
- H. Feng, C. Li and H. Shan, *Appl. Clay Sci.*, 2009, **42**, 439-445.
- F. Pan, X. Lu, Q. Zhu, Z. Zhang, Y. Yan, T. Wang and S. Chen, *J. Mater. Chem. A*, 2014, **2**, 20667-20675.
- M. Guisnet, P. Ayrault, C. Coutanceau, M. F. Alvarez and J. Datka, *Journal of the Chemical Society, Faraday Transactions*, 1997, **93**, 1661-1665.
- F. Ferreira Madeira, K. Ben Tayeb, L. Pinard, H. Vezin, S. Maury and N. Cadran, *Appl. Catal., A*, 2012, **443**, 171-180.
- F. Bonina, M. Giannossi, L. Medici, C. Puglia, V. Summa and F. Tateo, *Appl. Clay Sci.*, 2007, **36**, 77-85.
- T. Selvam, C. Aresipathi, G. T. Mabande, H. Toufar and W. Schwieger, *J. Mater. Chem.*, 2005, **15**, 2013-2019.
- L. H. Allen and E. Matijević, *J. Colloid Interface Sci.*, 1969, **31**, 287-296.
- L. H. Allen and E. Matijević, *J. Colloid Interface Sci.*, 1971, **35**, 66-76.
- E. G. Derouane, J. B. Nagy, Z. Gabelica and N. Blom, *Zeolites*, 1982, **2**, 299-302.
- Z. Gabelica, N. Blom and E. G. Derouane, *Applied Catalysis*, 1983, **5**, 227-248.
- R. Cai, Y. Liu, S. Gu and Y. Yan, *J. Am. Chem. Soc.*, 2010, **132**, 12776-12777.
- B. Zhang, Z. Zhong, K. Ding, Y. Cao and Z. Liu, *Ind. Eng. Chem. Res.*, 2014.
- S. E. Lattner, J. Sachleben, B. B. Iversen, J. Hanson and G. D. Stucky, *J. Phys. Chem. B*, 1999, **103**, 7135-7144.
- S. Kobatake, S. Takami, H. Muto, T. Ishikawa and M. Irie, *Nature*, 2007, **446**, 778-781.
- R. Demichelis, Y. Noël, P. D'Arco, L. Maschio, R. Orlando and R. Dovesi, *J. Mater. Chem.*, 2010, **20**, 10417-10425.
- T. Xue, Y. M. Wang and M. Y. He, *Microporous Mesoporous Mater.*, 2012, **156**, 29-35.
- E. G. Derouane, S. Determerrie, Z. Gabelica and N. Blom, *Applied Catalysis*, 1981, **1**, 201-224.
- V. N. Romannikov, V. M. Mastikhin, S. Hočevar and B. Držaj, *Zeolites*, 1983, **3**, 311-320.
- A. Corma, M. Cambor, P. Esteve, A. Martinez and J. Perezpariente, *J. Catal.*, 1994, **145**, 151-158.
- W. L. Wang, B. J. Liu and X. J. Zeng, *Acta Phys.-Chim. Sin.*, 2008, **24**, 2102-2107.
- D. Liu, C. Yao, J. Zhang, D. Fang and D. Chen, *Fuel*, 2011, **90**, 1738-1742.
- N. Y. Topsøe, K. Pedersen and E. G. Derouane, *J. Catal.*, 1981, **70**, 41-52.
- G. Tonetto, J. Atias and H. De Lasa, *Appl. Catal., A*, 2004, **270**, 9-25.
- A. S. Al-Dughaiter and H. de Lasa, *Ind. Eng. Chem. Res.*, 2014.
- I. M. Dahl and S. Kolboe, *J. Catal.*, 1994, **149**, 458-464.
- I. M. Dahl and S. Kolboe, *J. Catal.*, 1996, **161**, 304-309.
- D. Lesthaeghe, A. Horré, M. Waroquier, G. B. Marin and V. Van Speybroeck, *Chemistry-A European Journal*, 2009, **15**, 10803-10808.
- J. F. Haw, W. Song, D. M. Marcus and J. B. Nicholas, *Acc. Chem. Res.*, 2003, **36**, 317-326.

-
46. A. Corma, *Chem. Rev.*, 1995, **95**, 559-614.
47. G. Zhao, J. Teng, Z. Xie, W. Jin, W. Yang, Q. Chen and Y. Tang, *J. Catal.*, 2007, **248**, 29-37.
48. C. D. Chang, C. T. Chu and R. F. Socha, *J. Catal.*, 1984, **86**, 289-
5 296.
49. A. J. Foster, J. Jae, Y.T. Cheng, G. W. Huber and R. F. Lobo, *Appl. Catal., A*, 2012, **423**, 154-161.
50. P.H. Chao, H.W. Lin, C.H. Chen, P.-Y. Wang, Y.-F. Chen, H.-T. Sei and T.C. Tsai, *Appl. Catal., A*, 2008, **335**, 15-19.

10



Highly crystalline HZSM-5 zeolite was directly synthesized through steam assisted conversion (SAC) approach by using layered kaolin as raw materials, $\text{NH}_3 \cdot \text{H}_2\text{O}$ as alkali vapor source at the bottom of the teflon.